Biometals (2011) 24:477–487
DOI 10.1007/s10534-011-9410-0

In silico modeling of the Menkes copper-translocating P-type ATPase 3rd metal binding domain predicts that phosphorylation regulates copper-binding

N. A. Veldhuis · M. J. Kuiper · R. C. J. Dobson · R. B. Pearson · J. Camakaris

Received: 6 December 2010 / Accepted: 6 January 2011 / Published online: 22 January 2011

Abstract The Menkes (ATP7A) P_{1B}-type ATPase is a transmembrane copper-translocating protein. It contains six similar high-affinity metal-binding domains (MBDs) in the N-terminal cytoplasmic tail that are important for sensing intracellular copper and regulating ATPase function through the transfer of copper between domains. Molecular characterization of copper-binding and transfer is predominantly dependent on NMR structures derived from *E. coli* expression systems. A limitation of these models is the exclusion of post-translational modifications. We have previously shown that the third copper-binding domain, MBD3, uniquely contains two phosphorylated residues: Thr-327, which is phosphorylated only in the presence of elevated copper; and Ser-339, which is constitutively phosphorylated independent of copper levels. Here, using molecular dynamic simulations, we have incorporated these phosphorylated residues into a model based on the NMR structures of MBD3. Our data suggests that constitutively phosphorylated Ser-339, which is in a loop facing the copper-binding site, may facilitate the copper transfer process by exposing the CxxC copper-binding region of MBD3. Copper-induced phosphorylation of Thr327 is predicted to stabilize

N. A. Veldhuis and M. J. Kuiper contributed equally to this work.

N. A. Veldhuis
Department of Pharmacology, The University of Melbourne, Melbourne, VIC 3010, Australia

N. A. Veldhuis (✉) · J. Camakaris (✉)
Department of Genetics, The University of Melbourne, Melbourne, VIC 3010, Australia
e-mail: nveld@unimelb.edu.au

J. Camakaris
e-mail: j.camakaris@unimelb.edu.au

M. J. Kuiper
Victorian Partnership of Advanced Computing, Carlton, VIC 3053, Australia

R. C. J. Dobson
Department of Biochemistry and Molecular Biology, Bio21 Molecular Science and Biotechnology Institute, Melbourne, VIC 3010, Australia

R. C. J. Dobson
Biomolecular Interaction Centre, School of Biological Sciences, University of Canterbury, Private Bag 4800, Christchurch, New Zealand

R. B. Pearson
Peter MacCallum Cancer Centre, East Melbourne, VIC 3000, Australia

R. B. Pearson
Department of Biochemistry and Molecular Biology, The University of Melbourne, Melbourne, VIC 3010, Australia

this change in conformation. This offers new molecular insights into how cell signaling (phosphorylation) can affect MBD structure and dynamics and how this may in turn affect copper-binding and thus copper-translocation functions of ATP7A.

Keywords Menkes copper-translocating P-type ATPase · ATP7A · Metal-binding domain 3 · Molecular dynamics · Phosphorylation

Introduction

The low redox potential of copper (Cu(I) in the cell) is essential for many biological processes and its bio-availability is tightly controlled. The regulation of Cu(I) bio-availability ensures correct delivery to Cu(I)-dependent enzymes and prevents oxidative damage in elevated Cu(I) conditions. Following uptake by the Ctr1 channel, the key Cu(I) distribution pathway in humans involves transport by the cytosolic Atox1 copper chaperone and Cu(I)-translocation by the transmembrane Menkes (ATP7A) and Wilson (ATP7B) Cu-translocating ATPases (Cu-ATPase hereafter). These two P_{1B}-type ATPases deliver Cu(I) to cuproenzymes in the secretory pathway or facilitate Cu(I) efflux at the plasma membrane when intracellular levels are elevated and this involves highly regulated copper-responsive intracellular trafficking processes that are linked to Cu-ATPase activity (Braiterman et al. 2009; Greenough et al. 2004; Guo et al. 2005; Petris et al. 2002; Voskoboinik et al. 2003).

ATP7A and ATP7B share 69% sequence identity and contain eight transmembrane domains in addition to multiple intracellular loops, which are required for ATP binding, hydrolysis and Cu(I) translocation (Kaplan and Lutsenko 2009; Voskoboinik et al. 2003). General mechanisms for Cu-ATPase function are known, yet detailed aspects of structure and regulation remain unclear, including the role of protein phosphorylation in regulating Cu(I) bio-availability. Hormonal stimuli and other Cu(I)-independent pathways are known to regulate Cu-ATPase function (reviewed by Veldhuis et al. 2009a) and hence, cell signaling may be central to the interplay between protein–protein interactions and Cu(I) coordination chemistry pathways.

The N-terminal tail of human Cu-ATPases comprises ~44% of the total protein sequence length and also contains the major sites for regulation, via six homologous metal-binding domains (MBD1–6, Fig. 1a). These domains each contain an invariable CxxC Cu(I)-binding site (where x is any residue, see Fig. 1b, c) and all demonstrate a similar ability to receive Cu(I) from the Atox1 chaperone or by inter-domain Cu transfer between the MBDs (Banci et al. 2007; Strausak et al. 2003; Yatsunyk and Rosenzweig 2007). Each domain is ~72 amino acid residues in length and forms a ferredoxin-like fold ($\beta\alpha\beta\beta\alpha\beta$), with the CxxC Cu-binding motif located in the loop region between α_1 and β_2 (Fig. 1b). The MBDs are separated by linker regions of varying length and show significant sequence and structural homology to the Atox1 Cu(I) chaperone (Arnesano et al. 2002).

In the homologous yeast Ccc2 Cu-ATPase, two metal domains are present and these are essential for receiving Cu(I) and Cu(I)-transport activity (Morin et al. 2009). In the mammalian ATP7A/B proteins the equivalent domains, MBD5 and MBD6, are sufficient for Cu transport activity and Cu(I)-responsive intracellular protein trafficking (Cater et al. 2004; Strausak et al. 1999). Hence, the physiological importance of the conservation of six N-terminal Cu-binding domains in mammalian Cu-ATPases is unclear and has been the cause of continued debate (Banci et al. 2010a). There is speculation that mechanisms have evolved to sense low Cu(I) concentrations and/or carefully regulate Cu(I) transfer through the activated ATP7A/B channel (Banci et al. 2007; Forbes et al. 1999; Huster and Lutsenko 2003; Voskoboinik et al. 2001). Both of these processes are affected by the transfer of Cu(I) between domains and receiving Cu(I) from the Atox1 chaperone. In the ATP7B Cu-ATPase, for example, mutagenesis of CxxC motifs to prevent Cu-binding in specific domains affects domain packing and the Atox1-dependent Cu(I) delivery process to other domains, suggesting that "cross-talk" exists between domains. Interestingly, MBD3 Cu-interactions are predicted to be crucial for this process (LeShane et al. 2010).

The 3rd metal binding domain (MBD3) of ATP7A is considered the most differentiated in sequence and structure and has a lower affinity for Cu(I) than other MBDs and Atox1 (Banci et al. 2006a, 2010b). When receiving Cu(I), NMR studies show no detectable metal-bridged adduct between MBD3 and its physiological partner, Atox1. Thus, the current model suggests that Cu(I)-interactions in the MBD3 domain may only occur in elevated Cu environments,

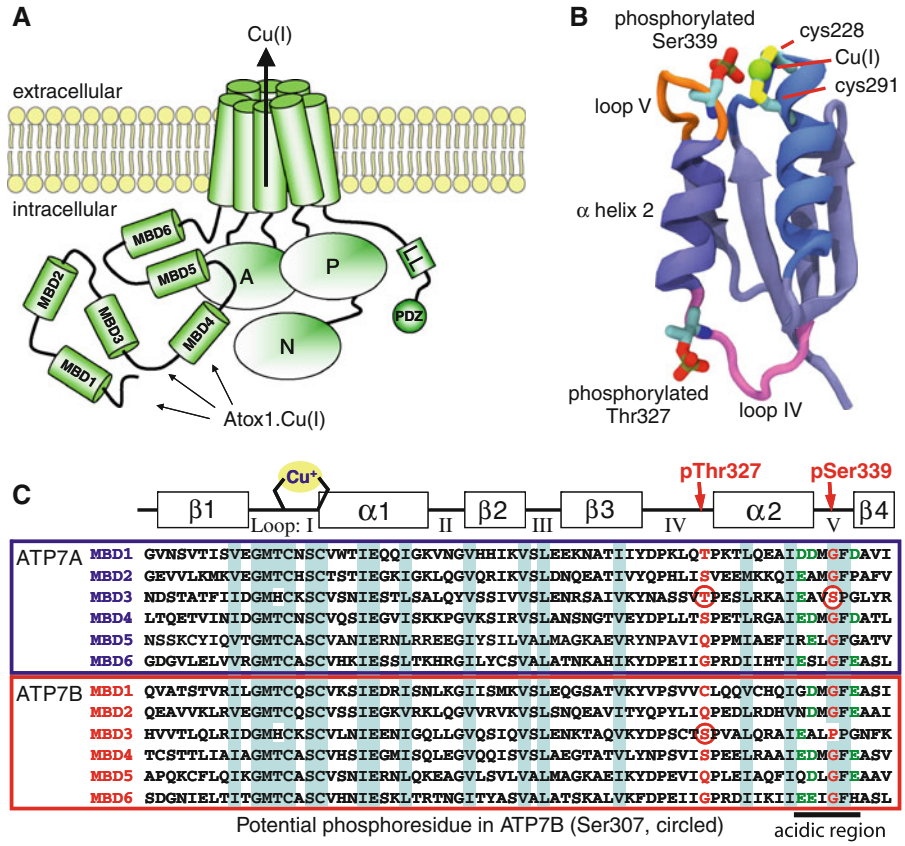

Fig. 1 **a** Molecular architecture of the Menkes Cu-ATPase and MBD3. Atox1 Cu(I) chaperone can transfer Cu(I) to one of six MBDs in the N-terminus. Other key domains/motifs for Cu-ATPase activity and trafficking are shown in the cytoplasmic loops and C-terminus. **b** NMR solution structure of MBD3 shows key regions for this study, including the Cu-binding site (Cys228, Cys291), loop IV (*purple*), loop V (*orange*) and phosphorylated residues, as labeled. **c** Sequence alignment of the MBDs in human ATP7A and ATP7B highlights amino acid conservation (shaded *blue*) and the residues found to be phosphorylated in MBD3 of ATP7A (*red* circles), relative to the secondary structure [adapted from Rodriguez-Granillo et al. (2009) and Arnesano et al. 2002]

providing a signal to trigger regulatory events and Cu(I) trafficking (Banci et al. 2006b).

MBD3 maintains the same $\beta\alpha\beta\beta\alpha\beta$ fold, yet it has only ~32% sequence identity to the other MBDs, resulting in some variation in the domain architecture (Banci et al. 2006a) and suggesting a specialized function. In particular, NMR studies revealed that the 5th loop joining $\alpha 2$ and $\beta 4$ (loop V in Fig. 1b) is longer in MBD3 when compared to the other domains. It also lacks a phenylalanine residue that is thought to stabilize the Cu-binding site by forming a network of hydrophobic contacts in the domain core. Instead, a downstream tyrosine (Tyr343) performs this role (Banci et al. 2006a, 2008).

Using cultured polarized epithelial cells (MDCK) we recently identified twenty phosphorylation sites in the N- and C-terminal cytosolic regions of human ATP7A, many of which are believed to be important for regulating ATP7A function (Veldhuis et al. 2009b). Intriguingly, more than half of these modified residues were located within, and surrounding, MBD3, suggesting that this is an important domain for regulating ATP7A via cell signaling pathways. Ser339 was phosphorylated in ATP7A protein purified from both low and elevated Cu(I) environments, indicating constitutive phosphorylation, at least in polarized MDCK cells. With the exception of MBD3, all other MBDs in ATP7A possess a glycine equivalent to residue 339 (Fig. 1c), indicating that Ser339 phosphorylation may provide a unique structural role for MBD3, yet the functional significance of this is unclear. In contrast, Thr327 was phosphorylated only

in copper-treated ATP7A samples, indicating a response to elevated Cu(I) concentrations (Veldhuis et al. 2009b). Thr327 is, therefore, predicted to be the target of a Cu(I)-specific signaling cascade. Interestingly, the equivalent residues in other MBDs of ATP7A are conserved as serine or threonine residues (Fig. 1c). Phosphorylation of ATP7B (Bartee et al. 2009) has also been observed and although specific sites were not identified, the conservation of a possible phosphorylation site in MBD3 of ATP7B (Ser307, Fig. 1) indicates the potential for similar cell signaling events to regulate ATP7B function.

Most of the ATP7A and ATP7B N-terminal MBD structures have been solved by NMR or X-ray crystallography using protein purified from bacterial expression systems (reviewed by Boal and Rosenzweig 2009). Such expression systems have many advantages, but are not always biologically relevant given the absence of relevant post-translational protein modifications, such as phosphorylation. Importantly, bacterial systems have yielded enough protein to determine a number of mammalian Cu(I) protein and domain structures (Achila et al. 2006; Anastassopoulou et al. 2004; Banci et al. 2010c; Dmitriev et al. 2006; Gitschier et al. 1998; Lamb et al. 2000; Wernimont et al. 2000) and supported our current understanding of the thermodynamics of Cu(I) binding and the Cu(I)-transfer process between purified Atox1 and MBDs (Banci et al. 2006b; Strausak et al. 2003).

To understand the role of phosphorylation in protein structure and function at the atomic level, computational methods have become increasingly utilized as a predictive tool and been shown to achieve a high level of accuracy by comparison with experimental data (Groban et al. 2006; Narayanan and Jacobson 2009). Others have employed protein dynamic simulations to further understand the molecular details of Cu(I) transfer processes between Atox1 and MBDs of ATP7B (Rodriguez-Granillo et al. 2009, 2010). Herein, we employ molecular dynamic (MD) simulations to elucidate the role of phosphorylation in the function of MBD3; in particular, how structural changes may influence Cu(I) binding. The data presented here predicts a model whereby constitutive phosphorylation of MBD3 at Ser339 increases accessibility of the CxxC Cu(I)-binding site and alters the electrostatic surface potential. Furthermore, the additional copper-induced phosphorylation of Thr327 is predicted to stabilize the structure and reduce these changes in conformation. These valuable insights challenge current understanding of MBD3 as the least likely domain to be metallated.

Methods

To investigate the role of phosphorylation of the 3rd metal binding domain (MBD3) of ATP7A, we employed MD simulations to systematically study the dynamics of apo- and Cu(I)-loaded MBD3 in various phosphorylation states (PDB entries 2G9O and 2GA7, respectively; Banci et al. 2006a). Our previous studies have shown that phospho-SerS339 (pS339) was observed under both low and elevated Cu(I) conditions, while phospho-Thr327 (pT327) was observed only in elevated Cu(I) (Veldhuis et al. 2009b). As such, the combination of simulations performed here reflect this phosphorylation data: phosphorylated Ser339 (pS339), with and without Cu(I); and phosphorylated Thr327 (pT327) with Cu(I) and including pS339. The variants constructed for the MD simulations are listed in Table 1.

Each model system was solvated with TIP3P water molecules to cube dimensions of 64 Angstroms with charge-neutralizing NaCl ions added to an effective concentration of 0.15 M using Visual Molecular Dynamics (VMD; Humphrey et al. 1996). Systems were optimized with a 200 picosecond equilibration with an NPT ensemble (constant number of particles, pressure of 1 atm and temperature of 310 K) followed by 70 ns of MDs simulation using a NVT ensemble (constant particles, volume and temperature). All simulations were performed with NAMD 2.7 (Phillips et al. 2005) on a Bluegene/P at the Victorian Life Sciences Computation Initiative (VLSCI). All simulations were run at a constant temperature 310 K, implemented with the Berendsen coupling scheme, using 12 Angstrom cutoffs, Particle Mesh Ewald (PME) electrostatics and the CHARMM forcefield (Brooks et al. 1983), with consideration of Cu–S bond and angle parameters (Holt and Merz 2007). Protonation states of all residues corresponded to those found at pH 7.

At the conclusion of the MDs simulations, trajectories were analyzed using the RMSDTT module within VMD to calculate structural root-mean square deviation (r.m.s.d.) of backbone heavy atoms (N, C_α and C). This indicates deviation of the backbone with reference to the average starting structure and was

Table 1 Combinations of MBD3 simulations undertaken in this work

Model	Phosphorylated residues	Cu(I)	Disulfide bond in Cu-binding loop
MBD3.Cu	–	Yes	–
MBD3.cys	–	No	–
MBD3.S–S	–	No	Yes
MBD3.Cu+p339	Ser339	Yes	–
MBD3.cys+p339	Ser339	No	–
MBD3.S–S+p339	Ser339	No	Yes
MBD3.Cu+pT327/pS339	Thr327 and Ser339	Yes	–

represented as a function of time for the duration of the simulation. The r.m.s. fluctuations (r.m.s.f.) measures the average backbone deviation *per residue* for the 70 ns simulation period.

Images were generated using the tachyon rendering module within VMD, while the electrostatic surfaces presented in Fig. 4 were calculated using Adaptive Poisson-Boltzmann Solver (APBS) (Baker et al. 2001).

Results

MD simulations of reduced and disulfide bonded MBD3 without Cu(I)

The NMR structure for apo-MBD3 (2G9O) contains reduced cysteines in the CxxC Cu(I)-binding site (Banci et al. 2006a). However, in nature there is the potential for reduced or disulfide-bonded cysteines to exist (Singleton et al. 2010). Thus initial simulations simply compared the apo-MBD3 with reduced cysteines (labeled "*cys*") with our modified disulfide bonded (labeled "*S–S*") Cu-binding site (see "Methods"). The backbone r.m.s.d. with respect to time showed that there was no significant conformational change in the backbone of the two unphosphorylated apo forms of MBD3 over the period of the MD simulations, despite the initial increase in r.m.s.d. of *MBD3.cys* (*MBD3.cys* and *MBD3.S–S*; Fig. 2a, red and purple lines). By measuring total fluctuations of individual amino acids (Fig. 2b), the constraints of the disulfide bridge were seen to reduce movement of *MBD3.S–S* in the Cu-binding loop. In addition, *MBD3.S–S* showed reduced movement in the loop between $\alpha 2$ and $\beta 4$ (loop V), where phosphorylation of Ser339 occurs. The slightly higher r.m.s.d. values for the simulations (Fig. 2a, c) are due primarily to the large fluctuations in the Cu(I) binding loop and the C-terminal, which is especially dynamic.

To judge the quality of the simulations, we directly compared the averaged structure from the *MDB3.cys* simulation to the averaged structure from the NMR ensemble 2G9O (Fig. 3). The average NMR structure [generated from an ensemble of the 30 best structures consistent with the distance restraints (Banci et al. 2006a)] was aligned with the average structure of *MDB3.cys* over 70 ns (50 structures, evenly distributed). The r.m.s.d. for the overlay of the α-carbons is 1.5 Å (Fig. 3a). We also examined regions of the backbone that show greater dynamics in each structure (Fig. 3b, c). Both our simulated average structure and the NMR ensemble show increased dynamics at the C- and N-terminal regions, along with the CxxC-containing loop I. Interestingly, loop IV of the NMR ensemble structure has increased r.m.s.d. values, compared to our simulation. Overall, our MD simulation for apo-MBD3 agrees well with the experimentally determined structure and validates our approach.

MD simulations of Ser339 phosphorylated MBD3 in the absence and with bound Cu(I)

To probe the effect of phosphorylation at position Ser339, we conducted MD simulations including phosphor-MBD3, modified *in silico* by replacing the hydroxyl group with a hydrated phosphate group, and compared these to the *MBD3.cys* or *MBD3.Cu* simulations (Fig. 2). Irrespective of the oxidation state of conserved cysteines, phosphorylation of residue Ser339 of MBD3 in the absence of Cu(I) significantly increased backbone movement (Fig. 2a, green and yellow lines). The most noticeable r.m.s.d.

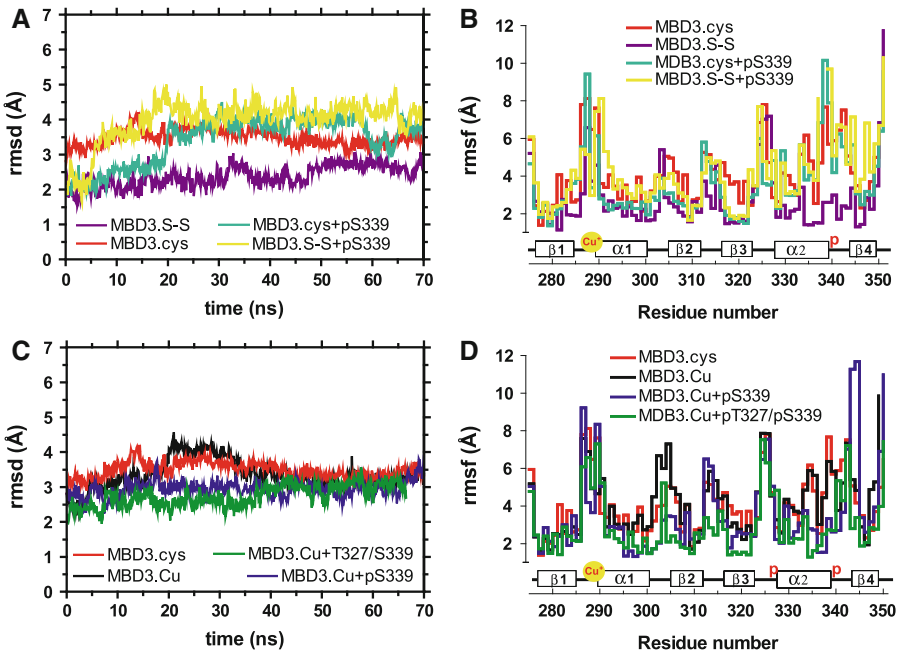

Fig. 2 As a measure of protein stability for whole domain over a 70 ns simulation, the backbone movement of heavy atoms (N, C_α and C) was calculated (r.m.s.d. in angstroms, with respect to initial structure) for phosphorylated or unphosphorylated apo-MBD3 (**a**) or Cu-MBD3 (**c**). To determine regions of the domain that contribute to changes in conformational dynamics, the average fluctuations (r.m.s.f. in Angstroms, average for total 70 ns) of backbone heavy atoms were determined for each residue, for apo-MBD3 (**b**) and Cu-MBD3 (**d**) with or without phosphorylation. The secondary structure and locations of the Cu-binding and phosphorylation sites are indicated (**b**, **d**)

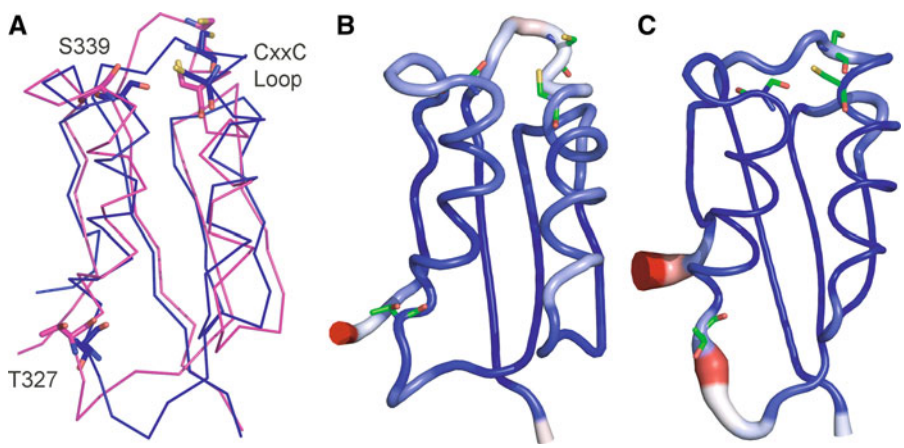

Fig. 3 **a** overlay of the averaged NMR ensemble, generated from pdb entry 2G9O (*blue*) and the averaged structure over the *MBD3.cys* simulation (*magenta*). The cysteines in the Cu(I) binding loop and the phosphorylated residues are indicated. **b** A putty representation of the backbone showing the r.m.s.d. for the α-carbon atoms in the averaged structure from the *MBD3.cys* simulation. **c** A putty representation of the backbone showing the r.m.s.d. for the α-carbon atoms in the averaged structure from the 30 NMR structures in 2G9O that agree with the distance restraints. For both b and c, the color scheme represents an increase in r.m.s.d of 0 Å (*blue*) to 5 Å (*red*) and the extent of the dynamics is demonstrated by the thickness of the ribbon

variation between phosphorylated and unphosphorylated forms was observed between *MBD3.S–S+p339* and *MBD3.S–S* (Fig. 2a, yellow and purple lines). Excluding the C-terminal tail, the greatest amino acid movement was evident in the phosphorylated loop V residues Val338 and phosphorylated Ser339 (Fig. 2b, yellow and green lines). Despite the lower r.m.s.d. values in *MBD3.cys+pS339*, the r.m.s.f. values for Val338 and Ser339 residues indicate similar movement in loop V for both apo forms of MBD3, when phosphorylated (Fig. 2b).

We then performed the same r.m.s.d. measurements for the MD simulations of Cu-bound MBD3 (*MBD3.Cu*; Fig. 2c, d). The r.m.s.d. values for Cu(I)-loaded MBD3 compared to apo-MBD3 (Fig. 2c, black and red lines) revealed similar conformational fluctuations when Cu(I) is bound to the protein. Cu-MBD3 simulations were performed with singly phosphorylated Ser339 or a doubly phosphorylated domain (pSer339 and pThr327). Overall, the greatest backbone movement was observed in *MBD3.Cu+pS339* (Fig. 2c, blue line).

MD simulations of phosphorylated Ser339 and Thr327 MBD3 with bound Cu(I)

In contrast, MD simulations of *MBD3.Cu+pT327/pS339* show that including a second phosphorylated residue in loop IV influences the domain dynamics by reducing backbone flexibility for most of the simulation period (Fig. 2c, *green* line). The r.m.s.f. measurements of the residues, in particular, show increased movement of Tyr343 and Arg344 of loop V in *MBD3.Cu+pS339* (Fig. 2d, *blue* line) compared to *MBD3.Cu+pT327/pS339* (Fig. 2d, *green* line), which indicates that a second phosphorylation event at Thr327 ameliorates the movement of these residues. Together the MD simulations suggest that Ser339 phosphorylation alters the dynamics of the domain by increasing backbone flexibility, independently of its Cu status. The addition of phosphorylation at Thr327 reduces this flexibility in Cu-bound MBD3.

Comparison of MD simulations reveals increased dynamics in loop V

To investigate the extent of the increased movement in loop V, we have superimposed the MBD3 starting structure and the structure after 70 ns. A coloring scheme was included to match r.m.s.f. values and indicate backbone regions with greatest flexibility (Fig. 4). To complement our experimentally determined phosphorylation data, comparative models show the extent of flexibility in the *MBD3.cys+pS339*, *MBD3.Cu+pS339*, and *MBD3.Cu+pT327/pS339* MD simulations. Loop V, which contains pS339, faces the Cu binding loop and, in the absence of phosphorylation it maintains a stable conformation. In contrast, phosphorylation of loop V facilitates a major shift in the solubility of the region, independently of the status of the Cys residues (Fig. 4a). The extent of the destabilization of the loop is also evident in the unraveling of the adjacent $\alpha 2$ helix and is associated with a larger solvent accessibility of the phosphoserine. This clearly shows exposure of the Cu-binding site, which may be important for Atox1 interactions. The high r.m.s.d. values for Val338 and phosphorylated Ser339 also coincide with increased backbone movement in loop IV, at the bottom of the model, where Thr327 is located.

For *MBD3.Cu+pS339,* the presence of the Cu(I) ion reduces movement of the $\alpha 2$ helix and phospho-Ser339 in loop V, compared to apo-MBD3 (Fig. 4b). Interestingly, movement still occurs in loop V, closer to the $\beta 4$ strand (*red* coloring in loop V, Fig. 4b) and suggests that the tendency for movement of Ser339 may be reduced by interaction between the phosphorylated group and the coordinated Cys-Cu-Cys, possibly electrostatic. Consistent with r.m.s.d. calculations in Fig. 2, fluctuations in the backbone are shown to be even further reduced in the doubly phosphorylated simulation (Fig. 4c). This reduction in dynamics suggests a stabilizing role for the phosphorylated MBD3 domain at both Thr327 and Ser339.

Electrostatic changes at surface of MBD3 upon phosphorylation

Given that electrostatic forces on the domain surface are important for interactions between Atox1 and MBDs of ATP7A (Banci et al. 2009), we examined the electrostatic surface potential of MBD3, with and without phosphorylation at positions Thr327 and Ser339. Atox1 has a largely positive surface and interacts with the yeast Cu-ATPase Cu-binding domain, Ccc2a, via charge complementarity with four negatively charged residues in loop V and $\beta 4$

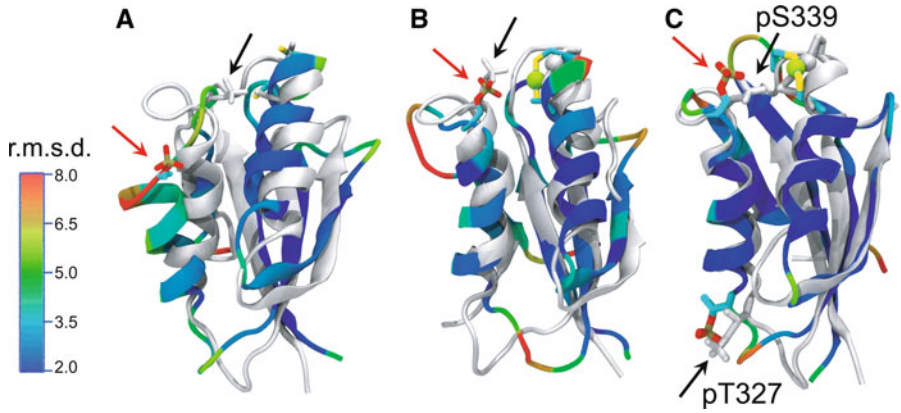

Fig. 4 Domain dynamics for *MBD3.cys+p339* (**a**), *MBD3.Cu+p339* (**b**), and *MBD3.Cu+pT327/pS339* (**c**). The average r.m.s.f for individual residues was calculated for each 70 ns simulation, as shown in Fig. 2. Representative images at 0 ns (*grey*) and 70 ns (*colored*) were superimposed and illustrate the extent of domain movement for apo-MBD3+pS339 (**a**), MBD3.Cu+pS339 (**b**) and MBD3.Cu+pT327+pS339 (**c**). The color scheme represents r.m.s.d. values (see color scale, *left*) and illustrates backbone heavy atom (N, C_α and C) movement. Phosphorylation groups are represented as *red* (oxygen) and *brown* (phosphorus) ball and sticks and their position after 70 ns is indicated by *red* arrows. *Black* arrows point to phosphorylation groups at 0 ns, to highlight the degree of movement after 70 ns

(Banci et al. 2006a). Comparing electrostatic models of the Cu-MBD3 in the presence of Ser339 phosphorylation highlights the change in charge distribution provided by the phospho-group (Fig. 5) and demonstrates a significant increase in negative charge in the Cu-binding region. Thus, at physiological pH, the surface of the Cu-binding region may have increased negative character due to the phosphoserine side chain. The other human Cu-ATPase domains have no more than three acidic residues within loop V (Fig. 1c). Our data suggest that when phosphorylated, MBD3 has a comparable charge status in loop V to that of other Cu-ATPase domains.

Discussion

Studies on the metallochemistry and thermodynamics of MBD3 in the copper transporter ATP7A using *E. coli* expression systems demonstrate the peculiarities of MBD3 with respect to the other N-terminal MBDs.

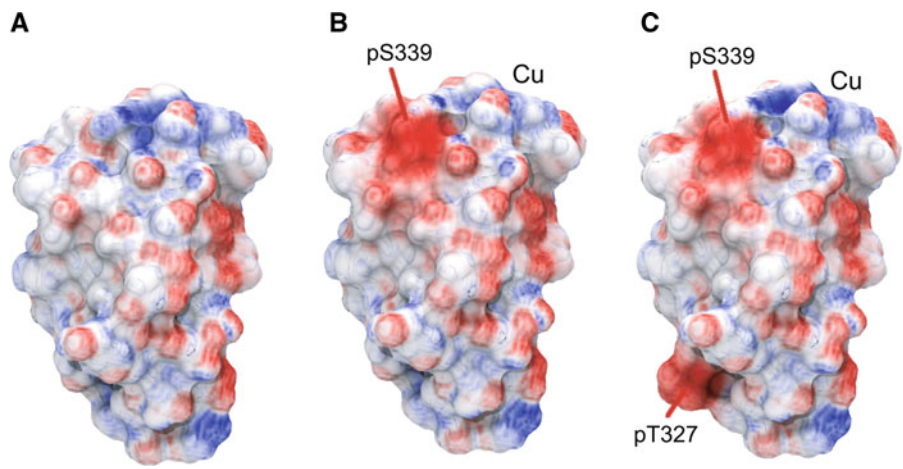

Fig. 5 Phosphorylation alters the MBD3 electrostatic surface charge potential. Electrostatic potential of MBD3 was measured for apo-MBD3 with reduced cysteines (**a**), MBD3.Cu+pS339 (**b**) and MBD3.Cu+pT327+pS339 (**c**). Negatively charged, positively charged and neutral amino acid side chains are represented in *red*, *blue* and *white*, respectively

However, previous studies have not included physiologically relevant phosphorylation of MDB3, which may be required for interactions with other metal domains or Atox1.

Here we studied the dynamics of MBD3 with respect to Cu(I) binding and phosphorylation at two residues, Thr327 and Ser339. Conservative predictions from MD simulations suggest a localized destabilization effect in loop V of MBD3, coinciding with increased exposure of the facing loop I, which contains the CxxC Cu-binding site. A second phosphorylation event may play a stabilizing role or influence other properties of the domain. This implicates phosphorylation in the regulation of Cu-binding, which could have downstream implications for Cu-ATPase activity and ATP7A trafficking. In consideration of the current model, where MBD3 is only metallated under elevated Cu conditions to stimulate ATP7A activity and trafficking (Banci et al. 2006a), this elevated Cu(I) environment may activate a signaling cascade leading to MBD3 phosphorylation at Thr327 and up-regulation of Cu-ATPase function. This potentially occurs via stabilization of the domain to reduce conformational changes caused by constitutive Ser339 phosphorylation. Surface electrostatic changes may also regulate interactions with other binding partners to stimulate trafficking or Cu-ATPase activity. Further experimental investigation, including mutagenic studies is required to test this model.

Our work highlights the importance of physiological protein modifications in regulating ATP7A function and suggests that, when phosphorylated under physiological conditions, MBD3 may have similar electrostatic surface properties to other MBDs in ATP7A. The reasons for this are not clear, although, it is tempting to speculate that these phosphorylation events may be part of a switch mechanism, and/or allow MBD3 to exist within ATP7A in more than one state, to at least temporarily increase its potential for Cu(I) binding. The presence of a second "Cu only" phosphorylation event on Thr327 could also regulate such a Cu(I)-binding cycle as described above. Alternatively, Thr327 phosphorylation may play an important role in the core structure of MBD3, given the reduction in backbone movement.

We predict that phosphorylation influences electrostatic properties of MBD3 to positively regulate interactions (and Cu(I) transfer) between MBDs or Cu chaperones. Computational biology in other protein systems further suggest that the free solvation energy is much greater for the phosphoserine side chain than for the carboxyl group of acidic residues, and hence, phosphorylation can enhance localized solubility (Groban et al. 2006). This is consistent with our observation of the destabilization of loop V and suggests solvent accessibility to the negatively charged region of MBD3 may be equal to, or greater than, other N-terminal metal domains of ATP7A. Furthermore, the propensity for MBD3 to be phosphorylated is indicated by high confidence scores in mass spectrometry analyses of multiple phosphorylation sites in this region (Veldhuis et al. 2009b) and supports a model for MBD3 to be frequently exposed to kinases in the cell.

In summary, our study suggests that phosphorylation of MBD3 results in major changes in protein dynamics and localized surface charge. The N-terminal metal domains are potential regulatory sites for Cu(I)-responsive ATPase activity and protein trafficking, and this indicates a role for cell signaling in regulated binding of MBD3 to other protein partners by changing its electrostatic properties. Thus, phosphorylation needs to be considered when determining the biochemical properties of MBD3 specifically and ATP7A in general, including global Cu(I)-transfer processes from Atox1 and between individual domains.

Acknowledgments The authors were supported by a NHMRC project grant (NV, JC). R.B.P is supported by a NHMRC Senior Research Fellowship. RCJD acknowledges the CR Roper Fellowship fund for salary support. The authors are also grateful to the Victorian Life Science Computational Initiative (VLSCI), which dedicated computational time to this project.

References

Achila D, Banci L, Bertini I, Bunce J, Ciofi-Baffoni S, Huffman DL (2006) Structure of human Wilson protein domains 5 and 6 and their interplay with domain 4 and the copper chaperone HAM in copper uptake. Proc Natl Acad Sci USA 103:5729–5734

Anastassopoulou I, Banci L, Bertini I, Cantini F, Katsari E, Rosato A (2004) Solution structure of the Apo and copper(I)-loaded human metallochaperone HAH1. Biochemistry 43:13046–13053

Arnesano F, Banci L, Bertini I, Ciofi-Baffoni S, Molteni E, Huffman DL, O'Halloran TV (2002) Metallochaperones and metal-transporting ATPases: a comparative analysis of sequences and structures. Genome Res 12:255–271

Baker NA, Sept D, Holst MJ, McCammon JA (2001) The adaptive multilevel finite element solution of the Poisson-

Boltzmann equation on massively parallel computers. IBM J Res Dev 45:427–438

Banci L, Bertini I, Cantini F, DellaMalva N, Herrmann T, Rosato A, Wurthrich K (2006a) Solution structure and intermolecular interactions of the third metal-binding domain of ATP7A, the Menkes disease protein. J Biol Chem 281:29141–29147

Banci L, Bertini I, Cantini F, Felli IC, Gonnelli L, Hadjiliadis N, Pierattelli R, Rosato A, Voulgaris P (2006b) The Atx1-Ccc2 complex is a metal-mediated protein–protein interaction. Nat Chem Biol 2:367–368

Banci L, Bertini I, Cantini F, Della-Malva N, Migliardi M, Rosato A (2007) The different intermolecular interactions of the soluble copper-binding domains of the Menkes protein, ATP7A. J Biol Chem 282:23140–23146

Banci L, Bertini I, Cantini F, Rosenzweig AC, Yatsunyk LA (2008) Metal binding domains 3 and 4 of the Wilson disease protein: solution Structure and interaction with the copper(I) chaperone HAH1. Biochemistry 47:7423–7429

Banci L, Bertini I, Calderone V, Della-Malva N, Felli IC, Neri S, Pavelkova A, Rosato A (2009) Copper(I)-mediated protein–protein interactions result from suboptimal interaction surfaces. Biochem J 422:37–42

Banci L, Bertini I, McGreevy KS, Rosato A (2010a) Molecular recognition in copper trafficking. Nat Prod Rep 27: 695–710

Banci L, Bertini I, Ciofi-Baffoni S, Kozyreva T, Zovo K, Palumaa P (2010b) Affinity gradients drive copper to cellular destinations. Nature 465:645–648

Banci L, Bertini I, Cantini F, Inagaki S, Migliardi M, Rosato A (2010c) The binding mode of ATP revealed by the solution structure of the N-domain of human ATP7A. J Biol Chem 285:2537–2544

Bartee MY, Ralle M, Lutsenko S (2009) The loop connecting metal-binding domains 3 and 4 of ATP7B is a target of a kinase-mediated phosphorylation. Biochemistry 48: 5573–5581

Boal AK, Rosenzweig AC (2009) Structural biology of copper trafficking. Chem Rev 109:4760–4779

Braiterman L, Nyasae L, Guo Y, Bustos R, Lutsenko S, Hubbard A (2009) Apical targeting and Golgi retention signals reside within a 9-amino acid sequence in the copper-ATPase, ATP7B. Am J Physiol Gastrointest Liver Physiol 296:G433–G444

Brooks BR, Bruccoleri RE, Olafson BD, States DJ, Swaminathan S, Karplus M (1983) CHARMM - A program for macromolecular energy, minimization, and dynamics calculations. J Comput Chem 4:187–217

Cater MA, Forbes J, La Fontaine S, Cox D, Mercer JFB (2004) Intracellular trafficking of the human Wilson protein: the role of the six N-terminal metal-binding sites. Biochem J 380:805–813

Dmitriev O, Tsivkovskii R, Abildgaard F, Morgan CT, Markley JL, Lutsenko S (2006) Solution structure of the N-domain of Wilson disease protein: distinct nucleotide-binding environment and effects of disease mutations. Proc Natl Acad Sci USA 103:5302–5307

Forbes JR, Hsi G, Cox DW (1999) Role of the copper-binding domain in the copper transport function of ATP7B, the P-type ATPase defective in Wilson disease. J Biol Chem 274:12408–12413

Gitschier J, Moffat B, Reilly D, Wood WI, Fairbrother WJ (1998) Solution structure of the fourth metal-binding domain from the Menkes copper-transporting ATPase. Nat Struct Biol 5:47–54

Greenough M, Pase L, Voskoboinik I, Petris MJ, O'Brien AW, Camakaris J (2004) Signals regulating trafficking of Menkes (MNK; ATP7A) copper-translocating P-type ATPase in polarized MDCK cells. Am J Physiol Cell Physiol 287:C1463–C1471

Groban ES, Narayanan A, Jacobson MP (2006) Conformational changes in protein loops and helices induced by post-translational phosphorylation. PLoS Comput Biol 2:238–250

Guo Y, Nyasae L, Braiterman LT, Hubbard AL (2005) NH2-terminal signals in ATP7B Cu-ATPase mediate its Cu-dependent anterograde traffic in polarized hepatic cells. Am J Physiol Gastrointest Liver Physiol 289:G904–G916

Holt BTO, Merz KM (2007) Insights into Cu(I) exchange in HAH1 using quantum mechanical and molecular simulations. Biochemistry 46:8816–8826

Humphrey W, Dalke A, Schulten K (1996) VMD: visual molecular dynamics. J Mol Graph 14:33–38

Huster D, Lutsenko S (2003) The distinct roles of the N-terminal copper-binding sites in regulation of catalytic activity of the Wilson's Disease protein. J Biol Chem 278:32212–32218

Kaplan JH, Lutsenko S (2009) Copper transport in mammalian cells: special care for a metal with special needs. J Biol Chem 284:25461–25465

Lamb AL, Wernimont AK, Pufahl RA, O'Halloran TV, Rosenzweig AC (2000) Crystal structure of the second domain of the human copper chaperone for superoxide dismutase. Biochemistry 39:1589–1595

LeShane ES, Shinde U, Walker JM, Barry AN, Blackburn NJ, Ralle M, Lutsenko S (2010) Interactions between copper-binding sites determine the redox status and conformation of the regulatory N-terminal domain of ATP7B. J Biol Chem 285:6327–6336

Morin I, Gudin S, Mintz E, Cuillel M (2009) Dissecting the role of the N-terminal metal-binding domains in activating the yeast copper ATPase in vivo. FEBS J 276:4483–4495

Narayanan A, Jacobson MP (2009) Computational studies of protein regulation by post-translational phosphorylation. Curr Opin Struct Biol 19:156–163

Petris MJ, Voskoboinik I, Cater M, Smith K, Kim BE, Llanos RM, Strausak D, Camakaris J, Mercer JFB (2002) Copper-regulated trafficking of the Menkes disease copper ATPase is associated with formation of a phosphorylated catalytic intermediate. J Biol Chem 277:46736–46742

Phillips JC, Braun R, Wang W, Gumbart J, Tajkhorshid E, Villa E, Chipot C, Skeel RD, Kale L, Schulten K (2005) Scalable molecular dynamics with NAMD. J Comput Chem 26:1781–1802

Rodriguez-Granillo A, Crespo A, Wittung-Stafshede P (2009) Conformational dynamics of metal-binding domains in Wilson disease protein: molecular insights into selective copper transfer. Biochemistry 48:5849–5863

Rodriguez-Granillo A, Crespo A, Wittung-Stafshede P (2010) Interdomain interactions modulate collective dynamics of the metal-binding domains in the Wilson disease protein. J Phys Chem B 114:1836–1848

Singleton WCJ, McInnes KT, Cater MA, Winnall WR, McKirdy R, Yu Y, Taylor PE, Ke BX, Richardson DR, Mercer JFB, La Fontaine S (2010) Role of Glutaredoxin1 and Glutathione in regulating the activity of the copper-transporting P-type ATPases, ATP7A and ATP7B. J Biol Chem 285:27111–27121

Strausak D, La Fontaine S, Hill J, Firth SD, Lockhart PJ, Mercer JFB (1999) The role of GMXCXXC metal binding sites in the copper-induced redistribution of the Menkes protein. J Biol Chem 274:11170–11177

Strausak D, Howie MK, Firth SD, Schlicksupp A, Pipkorn R, Multhaup G, Mercer JFB (2003) Kinetic analysis of the interaction of the copper chaperone Atox1 with the metal binding sites of the Menkes protein. J Biol Chem 278:20821–20827

Veldhuis N, Gaeth A, Pearson R, Gabriel K, Camakaris J (2009a) The multi-layered regulation of copper translocating P-type ATPases. Biometals 22:177–190

Veldhuis NA, Valova VA, Gaeth AP, Palstra N, Hannan KM, Michell BJ, Kelly LE, Jennings I, Kemp BE, Pearson RB, Robinson PJ, Camakaris J (2009b) Phosphorylation regulates copper-responsive trafficking of the Menkes copper transporting P-type ATPase. Int J Biochem Cell Biol 41:2403–2412

Voskoboinik I, Mar J, Strausak D, Camakaris J (2001) The regulation of catalytic activity of the Menkes copper-translocating P-type ATPase—role of high affinity copper- binding sites. J Biol Chem 276:28620–28627

Voskoboinik I, Mar J, Camakaris J (2003) Mutational analysis of the Menkes copper P-type ATPase (ATP7A). Biochem Biophys Res Commun 301:488–494

Wernimont AK, Huffman DL, Lamb AL, O'Halloran TV, Rosenzweig AC (2000) Structural basis for copper transfer by the metallochaperone for the Menkes/Wilson disease proteins. Nat Struct Biol 7:766–771

Yatsunyk LA, Rosenzweig AC (2007) Cu(I) binding and transfer by the N-terminus of the Wilson disease protein. J Biol Chem 282:8622–8631